Gravitational wave detector derived error signals for the LIGO thermal compensation system

Rupal S Amin and Joseph A. Giaime

202 Nicholson Hall, Tower Road, Dept of Physics and Astronomy, Louisiana State University, Baton Rouge, LA 70803-4001
and
LIGO Livingston Observatory, P.O. Box 940, Livingston, LA 70754

E-mail: ramin@phys.lsu.edu

Abstract. Thermal lensing has been one of the sensitivity limiting factors for the LIGO detectors since their inception. Although estimates of such lensing was assumed when LIGO's core optics were specified, in practice a thermal lensing compensation system (TCS) was installed in 2004 in order to improve mode matching to the injected beam and ultimately detector sensitivity. This subsystem's primary purpose was to induce a corrective thermal lens in the input test mass mirrors or LIGO's 4 km Fabry-Perot arms. A few empirically-motivated means of monitoring the focal parameters of the input couplers were employed for the 2005-2007 science run, "S5." We discuss results of a numerical model study, a set of signals, "focal discriminants," that could have been used during S5 to set TCS compensation levels. Most of these signals would not have needed the installation of any new equipment or software. If investigated further, these "focal discriminants" may find utility in pathfinder projects as the next generation LIGO detectors is commissioned.

1. Introduction

The Laser Interferometer Gravitational-wave Observatory's (LIGO) objective is to detect and observe gravitational waves from distant astrophysical sources using interferometric distance measurements of mirrors serving as test masses separated by multiple-kilometers [1-3]. Between 2005 and 2007, LIGO's detectors operated with displacement sensitivity of 10^{-19} m/$\sqrt{\text{Hz}}$ at 100 Hz [3]. This was partially made possible through large circulating laser powers within the detectors. These power levels were sufficiently high to induce thermal lenses in the exceedingly low loss LIGO core optics (see figure 1). These core optics, however, were designed to be well mode matched for a particular input power and an assumed optical absorption in all optics, in particular especially the input test masses (ITMs) [4]. A well mode matched detector was expected to be more sensitive to gravitational waves than a lossy detector [5-7] ; here, "lossy" implies poor mode matching However, imbalances in ITM thermal lenses and overall suboptimal lensing reduced the detector sensitivity in shot noise limited frequency bands [4, 8-10]. Monitoring schemes explored through empirical correlation suggested signals that could parametrically track the average and differential ITM focal lengths. These "focal discriminant" signals were used to manually or automatically tune thermal (lensing) compensation systems (TCS) to provide optimum mode matching and therefore maximize displacement sensitivity. During the fifth science run, "S5," the LIGO detectors used this scheme successfully. Although various optical spatial phase-front measurement techniques have been studied to monitor focal error in LIGO-like detectors, there may be utility in having discriminants that are derived from radio frequency (RF) heterodyne quadratures or phase modulated RF sideband intensities. As a result, a simplified model of the detectors has been constructed and examined for new candidate signals. The stipulations for these models and resulting focal discriminants are noted in

following sections. These techniques, if simulated and qualified, on next generation detectors may serve as an intermediate or backup solution to TCS control schemes being designed.

2. **Description of LIGO Detector Array**

The LIGO detector array is comprised of three antennas (detectors) at two sites, Hanford, WA and Livingston, LA [2]. One large 4 km antenna was constructed at each site with a second half size unit situated within the Hanford installation. Each detector was designed as a multi-kilometer version of a power recycled Michelson interferometer with Fabry-Perot arm cavities. The optical topology for each 4 km detector is shown in figure 1.

The figure 1 details the six mirrors set in a power recycled Michelson interferometer formation, their pick off ports, and relevant radio frequency demodulation channels pertinent to this paper's simulations. The mirrors labeled ITMx and ETMx form the "x-axis" Fabry-Perot arm cavity; mirrors labeled ITMy and ETMy form the "y-axis" Fabry-Perot arm cavity. Here ITM refers to the input (coupler) test mass, and ETM refers to the end test mass (a fully reflective mirror). The recycling mirror (RM) forms the power recycled cavity (PRC) when paired with the ITMs. In the actual LIGO detectors, the ITMs and ETMs are stationed approximately 4 km apart from each other. The mirrors comprising the PRC are stationed approximately 9 m apart from each other. LIGO's operation at the dark Michelson fringe permits the interferometers to act as large composite resonators. The primary means of loss within the detectors were the mirrors' intrinsic losses, scattering and absorption.

A carrier beam and the primary RF phase modulated sidebands enter the detector through the RM. The primary RF sidebands resonate in the PRC. The sidebands allow LIGO to utilize a variant of the Pound-Drever-Hall type (PDH) length servo scheme [2, 3, 11]. Secondary RF sidebands are not resonant within the PRC and are therefore used in measuring the average size of the arm cavity via the retroreflected light. The sidebands are also used in a control servo to minimize alignment perturbations [2, 3, 12]. Optical pickoff ports within the interferometer provide a means to measure the relative position (and alignment) of the PRC and Fabry-Perot mirrors (see figure 1). During S5, the primary degree of freedom, differential arm motion or "DARM," is measured directly at the anti-symmetric (AS) port by heterodyning the AS light with the primary sideband modulation RF to form an error signal that is directly related to the

differential Fabry-Perot arm lengths as noted in section 4.4 of reference [3].

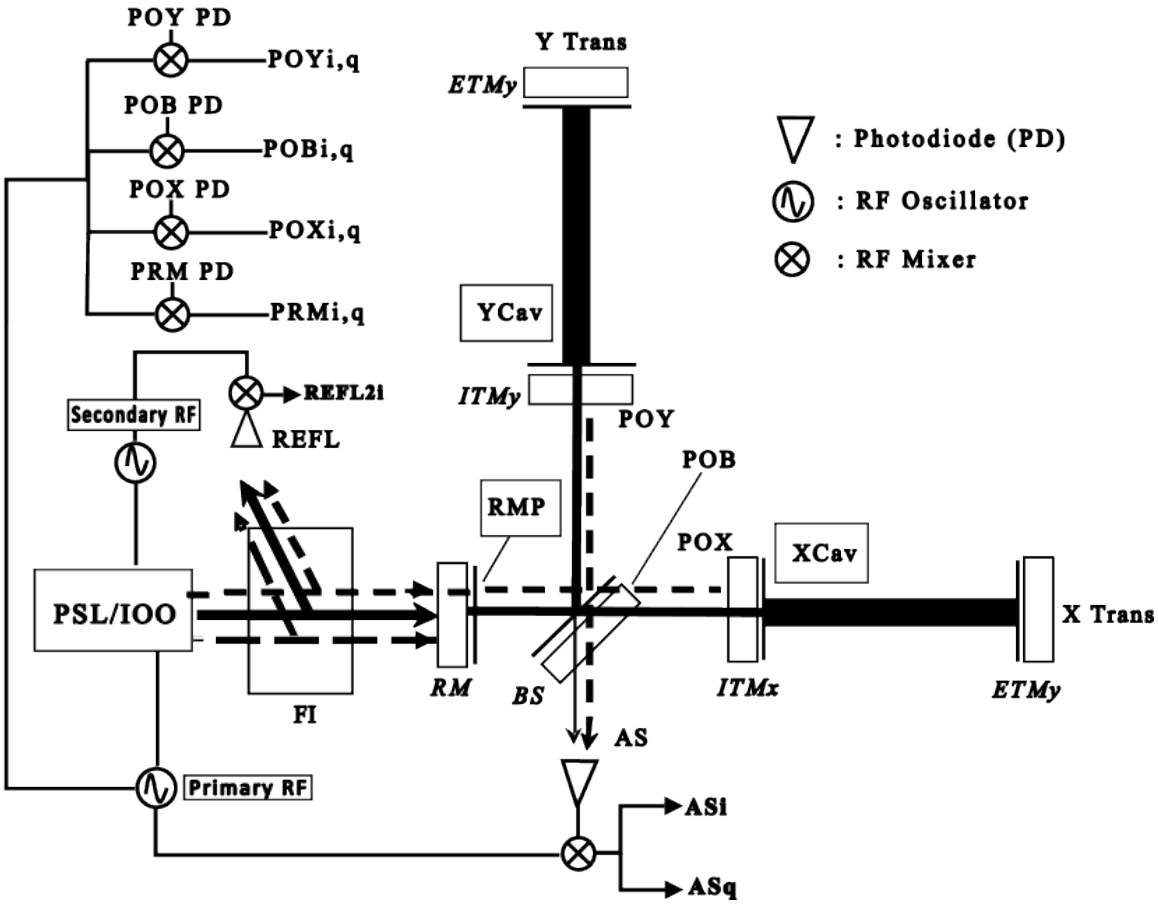

Figure 1: A schematic of the LIGO core optics. Optical pickoffs are noted in normal font. The mirrors are labeled in italic font. Vertical lines adjacent to mirrors indicate which side is highly reflective (HR). A carrier beam leaves the pre-stabilized laser and input/output optics (PSL/IOO) stage with phase modulated RF sidebands. The carrier and sidebands are incident on the recycling mirror's (RM) antireflective surface. The nonresonant secondary sidebands return upstream and are routed to the reflected port (REFL) by a Faraday isolator (FI). The primary sidebands resonate in the power recycled cavity (PRC) comprised of the two input test masses (ITMs), beamsplitter (BS), and the RM. The primary sideband light leaks out the antisymmetric (AS) port due to an asymmetry in the ITM to BS distance. The carrier resonates in both the arm cavities and the PRC. The arms' highly reflective end mirrors are labeled end test masses (ETMs). Light pickoff (PO) ports are drawn close to their nominal positions. The boxed pickoff ports (XCav, YCav, and RMP) are ports used for diagnostic purposes and signal fidelity. Here RMP refers to "Recycling Mirror Pickoff;" Xcav refers to "Internal X-Cavity Pickoff;" YCav refers to "Internal Y-Cavity Pickoff;" Primary and secondary RF oscillators in the lower left provided both RF excitations for phase modulations and demodulation at photodiode mixers. AS port light demodulated quadrature signals are shown. Demodulated signals are noted with their port name in capitals and the quadrature in lower case. Demodulated signals generated from the secondary RF are noted by a "2." Other demodulated signals are shown in the upper left for diagrammatic simplicity.

Each gravitational wave detector measures the projection of gravitational waves' strain as they pass through the detector. These projected strains alter arm lengths in each detector to a different degree based on polarization and sky position. Coherent DARM excitations between Hanford and Livingston that cannot be associated with environmental factors generate gravitational wave candidates. Local environmental noises typically generate incoherent differential arm motions between Hanford and Livingston. A more detailed description of LIGO's operation during 2005-2007 is documented in reference [3].

3. Description of the Problem

The DARM sensitivity loss caused by thermal lensing and other thermal aberrations in gravitational wave detectors has been described in past articles [2, 4, 8, 10, 13-17]. ITM thermal lensing results from non-uniform laser-induced temperature gradients changing local indices of refraction. The injected carrier beam and sidebands were designed to be optimally mode matched to the interferometers once the ITMs reached their steady state thermal load. The long-arm cavity's stability factor, g, varies less than one percent around 0.4 between cold and hot state. Cavity stability parameters, g, between 0 and 1 represent cavities capable of transversely confining laser light fields and selectively filtering intensity patterns (transverse modes). Therefore, the resonant carrier remained spatially confined on the fundamental Gaussian resonant mode.

The PRC's cold cavity stability parameter, however, is slightly greater than 1. The circulating light in such a cavity is not transversely contained. Subtle changes in the ITM focal length can readily change the primary sideband power accumulation, beam parameters, and pointing. This results from PRC light traversing thermal lenses in the ITM substrates. By contrast, carrier beam parameters are greatly influenced by the Fabry-Perot arm's mode dependent reflectivity. This suppresses carrier higher order modes and pointing drift. Measurements made by the Livingston commissioning team prior to TCS optimization demonstrated that the primary RF sidebands did not possess the same beam parameters as the carrier beam for a cold interferometer and did not remain coaxial to the carrier. These issues have been noted in references [2, 6, 14, 18].

The application of TCS stabilized the PRC for high power operation during S5 [3]. The LIGO TCS system is comprised of carbon dioxide lasers that project correction patterns on each ITM's highly reflective surface. Ideally, the TCS centrally heated the ITMs to induce a positive lens. This occurs prior to and during the main laser power ramp to operational powers during S5. The TCS central heating would gradually be reduced as a function of injected main laser power. When the positive thermal lensing became excessive, annular heating generated a counter temperature gradient (a negative lens) [4, 19].

During S5 and post-S5 operation, TCS tuning has been performed initially by looking at two primary signals. The beamsplitter pick off light demodulated at twice the primary RF frequency parametrically measured average or "common mode" ITM thermal lensing. This signal is called the "sideband power on the beamsplitter" (SPOB). Tuning the TCS to maximize SPOB improved detector stability at operating powers. AS port light demodulated in-phase with the primary modulation yielded a measure of differential lensing. Zeroing this signal corresponded to minimizing the differential thermal lensing. These signals were derived from the existing length sensing and control (LSC) signals. At Hanford, a second system was used to monitor the average (common) lensing via a segmented photodiode [4]. This system was based on the measuring RF beat notes that originate from the fundamental mode beating against the first excited circularly symmetric mode [20]. It was determined that the LIGO Livingston detector did not require a continuous control servo. Therefore, the second system installed at Hanford was not implemented at Livingston.

For both the S5 and later iterations of LIGO [21, 22] the advantage of having a defined, readily modeled, and readily available set of thermal lensing discriminants would benefit interferometer mode matching, stability, and ultimately strain sensitivity.

4. Model Description

To this end, a simplified optical model of the detector has been assembled for analysis. The model's design is based on a perfectly mode matched LIGO. The model layout mimics the Livingston detector's measurements. Both ETMs and the RM are set using as-built radii of curvature. Each ITM's radius of curvature is set to match the fundamental cavity mode set by RM and the ETMs. This method places the unperturbed model's baseline at the optimized physical solution.

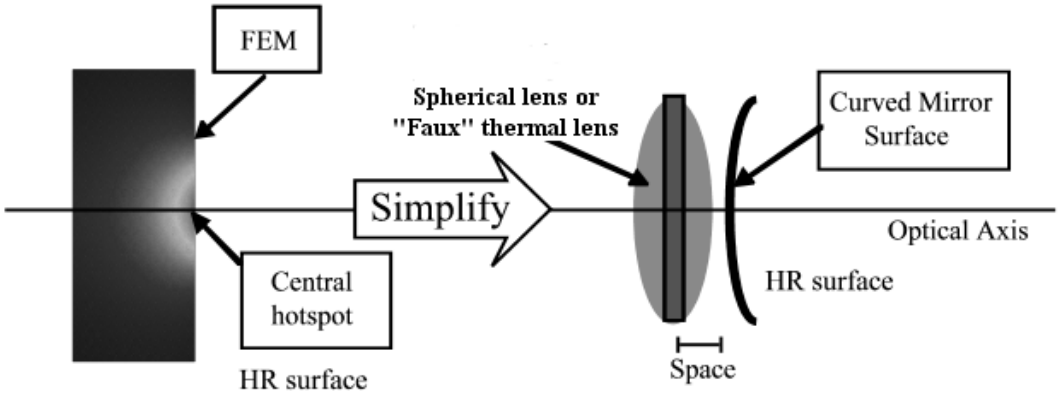

Figure 2: The simplification of thermal aberrations. A FEM simulation (left) demonstrates that the induced hot spot is situated adjacent the highly reflective surface. The faux thermal lens (right) places a spherical lens adjacent to a fixed highly reflective curved surface.

In the model, each ITM's thermally-induced distortion is represented by a spherical lens (figure 2). Spherical lenses can replicate 93 % of a thermal lens optical aberration [10, 23]. While the thermal lens can be simulated using finite element models (FEM), spherical lenses reduce the CPU and memory load required for each simulation. Through the rest of the paper, we refer to the spherical lenses as "faux" thermal lenses.

Mirror curvature change is not investigated in our model. For LIGO optics, the optical path length change due to thermal lensing is an order of magnitude larger than that caused by thermal expansion [9, 24]. FEM simulations indicate that the optical path length change on axis due to an ITM's thermal lensing was approximately 10^{-5} m. This assumes 1 W was incident on the RM; this yields approximately 5 kW incident on the ITMs' highly reflective surfaces. For comparison, the same FEM indicated that the thermal expansion of the mirror was approximately 10^{-6} m.

The S5 LIGO detectors represent the typical power recycled Michelson Fabry-Perot topology. Although the Enhanced LIGO detectors began data taking during the writing of this paper, the upgrades did not directly affect the layout shown in figure 1 [22].

The optical model was built using Frequency domain INterferomEter Simulation SoftwarE, FINESSE[1] [25-27]. This program is designed to examine rapidly the optical behaviour of gravitational wave

[1] www.gwoptics.org/finesse

detectors and interferometers in general. This precludes any mechanical additions such as suspensions and radiation pressure. It assumes that all beams behave in a Gaussian manner. Optics within this program are infinite in diameter and are ideally thin. Diffraction losses are not included in this program. Thick optics can be constructed by fitting a glass slab together with a curved surface. Unlike other interferometer simulation programs such as the FFT program used in reference [14], this program asks the user to determine how many transverse modes are to be used in a simulation. Light fields excited beyond this maximum mode number are lost.

The primary compromise of using FINESSE is its application of dead band servos. LIGO's detectors maintain core optic mirror spacings necessary for low-noise detection by use of four linear servo control loops. This simulation sets these spacings by iteratively altering mirror positions until a user specified optical error signal falls below a user defined threshold. A user specifies the interferometer parameter to be changed, its range, and the number of points to be plotted. FINESSE's locking servos re-optimize mirror positions for each parameter point from smallest to greatest value. The optical error signals specified were the same signals used in the S5-era LIGO detector. This algorithm mimics the behaviour of a simple control loop with an integrator. To simulate the length servo control loops, each length error signal's demodulation phase was carefully tuned to maximize response to its respective degree of freedom.

Since only two mirror aberrations are varied in the simulation, only two tests are required. The first changes both mirrors' ITM lenses by the same focal length, pure common mode lensing. The second test alters the focal length of ITM lenses by an equal but opposite amount, pure differential mode lensing. Both lensing simulations generate plots in units of diopters. Zero diopters in each plot indicates the point of perfect mode matching. Both simulations are run with a fixed amount of laser power (1 W) entering the RM.

5. Sorting Through Discriminants

The results from the simulations yield several candidates capable of monitoring focal lengths. Stipulations were constructed to narrow the number of possible candidates to viable candidates in the actual LIGO detectors.

1) The most important restriction requires signals to be acquired from light pickoff ports easily implemented in the LIGO detectors.
2) Although sensors that employ spatial phase measurement or that require gain measurements have been developed [4], in this work we seek simpler signals derived from DC light intensity, RF light intensity, or RF signal phase.
3) Both common and differential lensing signals must be usable in the presence of length sensing and control servo action. The length sensing and control system can correct small changes in optical phase delay induced by ITM motion. The focus discriminants must depend on ITM focal values only.
4) Discriminants are ideally linear with respect to their degree of freedom near the desired operating point. Signals that do not cross zero at perfect mode matching or non-linear need not be excluded in this study, since a linear TCS servo may not be necessary (see section 8).

6. Choosing the Focal Power Range

The plotting abscissa is chosen to cover focal powers from -2×10^{-4} diopters to 2×10^{-4} diopters. Here $1 \text{ diopter} = 1 \text{ m}^{-1}$. This focal power range is large enough to include carrier induced thermal lensing within the S5-era LIGO detectors, the S5-era TCS induced thermal lensing, and proposed post-S5 TCS lensing capacity.

The change in thermal lensing, f_{therm}, driven exclusively by carrier beam heating can be estimated by the following equation [27]:

$$f_{therm}(P_a) \approx \frac{\omega^2}{2\left(\frac{\beta P_a}{4\pi\kappa}\right)}.$$

Here β represents the thermo-refractive coefficient of fused silica; κ represents thermal conductivity; ω is the beam spot size on the ITM; and P_a represents the absorbed optical power. Using measured absorption ratios for the LIGO Livingston ITMs and the estimated large arm circulating power at nominal S5 operating power, the focal power change is approximately 4×10^{-5} diopters.

At an absolute focal power error of 5×10^{-5} diopters, the simulated interferometer power build up drops by one percent. The loss of power build up occurs because carrier and sideband power enters higher order modes not tracked by our simulation. Beyond this region our model loses integrity.

The S5-era TCS is capable of achieving an absolute focal power of approximately 1×10^{-4} diopters for annulus heating. Later iterations of LIGO proposed a TCS capable of generating focal powers at least 2×10^{-4} diopters. To cover both the S5 TCS actuation ranges and following iterations, the simulations were run from -2×10^{-4} diopters to 2×10^{-4} diopters.

7. Results

The set of candidates and their characteristics are summarized in table 1. Distinct patterns observed in the following candidates suggest a means of determining how TCS should heat the ITM pair to achieve optimized mode matching.

Table 1: Signal Candidates.

	Signal Candidate	Characteristics
#	(Common Mode)	
1	Beamsplitter Pickoff Light Double Demodulated at the Primary Sideband RF	Maximum excursion: 1.5 W at BS AR coating Slope near operating point: $\approx -4 \times 10^{-6} \frac{\text{W}}{\text{diopter}}$
2	Antisymmetric Port Secondary Sideband Light's TEM_{22} Mode	Maximum excursion: $10^{-4}\sqrt{\text{W}}$ Slope at operating point: 0 (zero) DC offset near operating point: 0
	(Differential Mode)	
3	Beamsplitter Pickoff Light Demodulated in Quadrature Phase with the Secondary Sideband RF	Maximum excursion: 10^{-3} W at BS AR coating Slope near operating point: $33.84 \frac{\text{W}}{\text{diopter}}$ DC offset near operating point: 1×10^{-5} W

A set of five graphs is shown for the RF based error signal candidates 1 and 3. The top subplot is the candidate signal in question as a function of focal power in diopter. The following subplots are of the error signal for LIGO's four length degrees of freedom: differential Fabry-Perot arm length, differential ITM/BS distance, average RM/ITM distance, and common Fabry-Perot arm length. The error signals associated with each degree of freedom are labeled as follows: ASq = "antisymmetric port light demodulated in quadrature at the primary sideband RF," POBq = "pickoff beamsplitter light demodulated in quadrature at the primary sideband RF, "RMPi" = "recycling mirror pickoff light demodulated in-phase at the primary sideband RF," and REFL2i = "reflected light demodulated in-phase at the secondary sideband RF," respectively. The numeric "2" refers to signals demodulated at the secondary sideband RF.

Since spherical lenses can mimic changes in interferometer length degrees of freedom. These error signals are plotted for the candidates to show the length servo signals in response to simulated lensing variation. The top graph in each case represents the candidate TCS error sensor signal in the reasonably realistic presence of interferometer length servo control. Signal strengths for candidates are measured at the core optic faces since losses due to the output relay optics are often difficult to predict accurately.

Signal Candidate 1

The first common mode candidate was motivated by prior use of SPOB to monitor the common lensing state of the LIGO detectors. The uppermost subplot in figure 3 indicates three maxima. Power variations in SPOB were correlated to the number of higher order modes in the PRC. The central maximum peak is situated -1×10^{-6} diopters from the point of perfect mode matching. A distinct global maxima (plateau) is positioned immediately to the right of perfect mode matching. The focal power of the closest "corner" is approximately 1×10^{-5} diopters. This places the end of the positive regime rise at the edge of our conservative threshold. This simulation suggests that the original protocol of maximizing SPOB to improve mode matching was incorrect. Instead, the point of perfect mode matching neighbors a minimum in the trace.

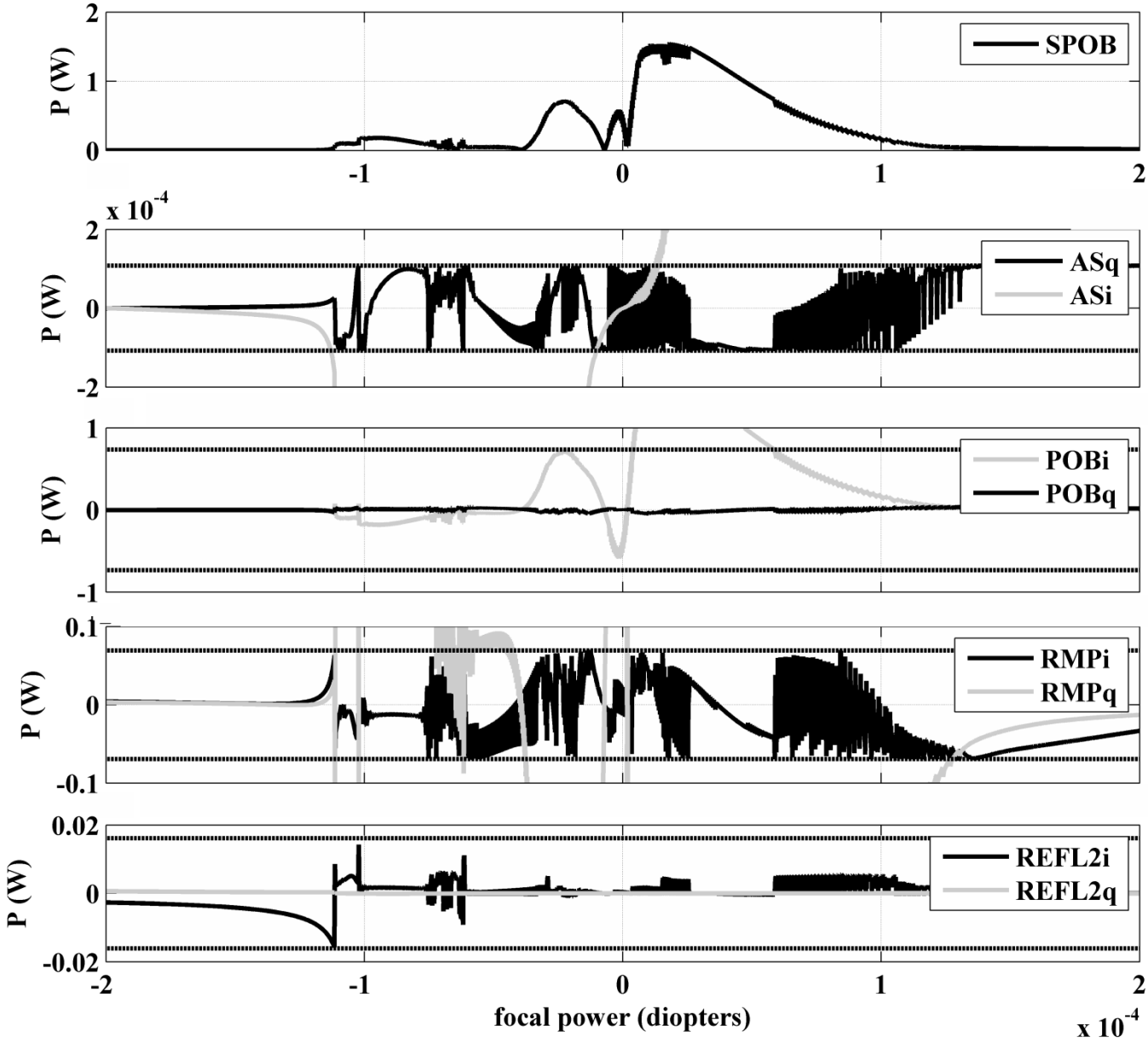

Figure 3: Common lensing signal candidate #1 and control signals. The top trace plots the behaviour of beamsplitter pickoff light doubly demodulated at the primary sideband modulation frequency (SPOB) as a function of common focal power. In the following traces, the letters "i" and "q" refer to in-phase demodulation and quadrature phase demodulation, respectively. The following traces, in order, correspond to the various degree of freedom error signals: ASq = differential arm control; POBq = the Michelson; RMPi = the common motion of the power recycling cavity; and REFL2i = the common motion of the arm cavities. The dotted lines correspond to the locking accuracy threshold or RMS motion of a specific length degree of freedom. The servos remain stable throughout the operating region from -5*10^{-5} diopters to 5*10^{-5} diopters. Through this region the amount of sideband power on the beamsplitter (SPOB) has two minima and three maxima. The minima at perfect mode matching, zero diopters, is due to the increasing number of modes contained within the PRC. Asymmetry in the SPOB around zero diopters is attributed to the asymmetries in the interferometer.

Signal Candidate 2

A second approach to monitoring common mode lensing technically violates the exclusion of wavefront sensors (figure 4). The heart of this candidate is the use of a non-degenerate optical spectrum analyzer to filter the Hermite-Gauss 22 mode of the secondary sideband light. While the intensity of this candidate is miniscule compared to the preceding candidates, it has a singular advantage. The ratio of the upper and lower secondary sidebands is unity at perfect mode matching.

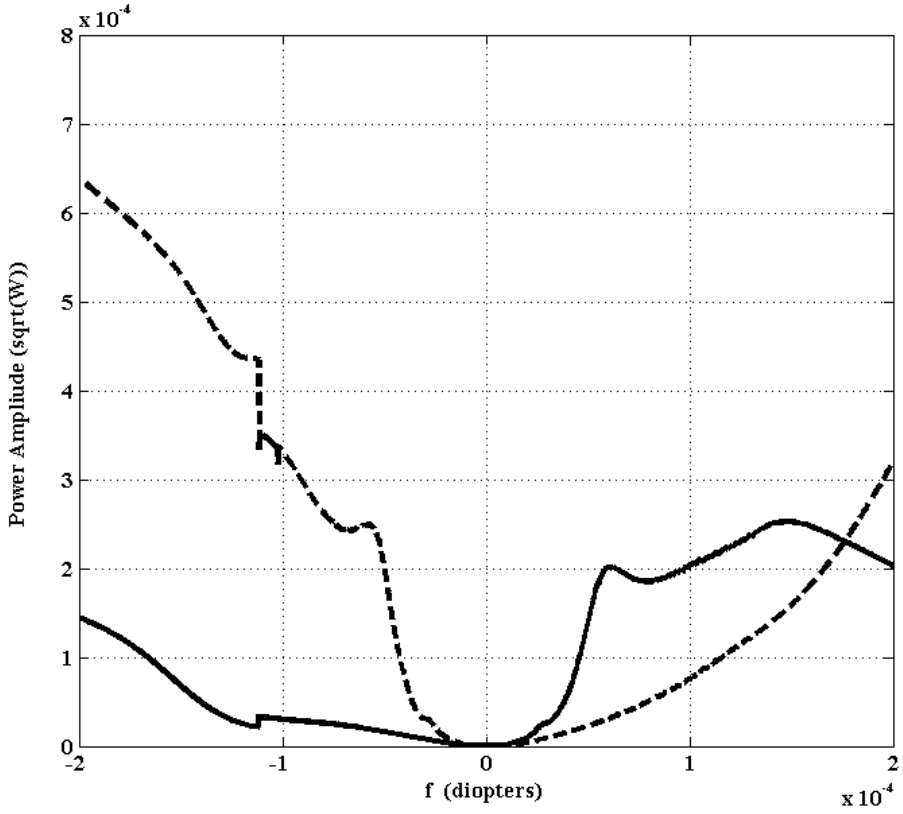

Figure 4: Common lensing simulation #2 is taken from the same simulation as figures 4. Traces represent the amplitude of the TEM_{22} mode of the POB light separated from the carrier by the secondary sideband modulation frequency. The black line represents the upper sideband; the dotted line represents the lower sideband. The advantage of this signal is clear as the two sidebands cross at perfect mode matching. However, small amplitudes of order $10^{-4}\sqrt{\mathrm{W}}$ imply the signal's lack of viability.

Signal Candidate 3

The differential signal is derived from beamsplitter pickoff light demodulated in quadrature phase with the secondary sideband RF (figure 5). Even though the secondary sideband was not intended to resonate within the PRC, leakage light does inevitably sample the thermal lenses in the ITMs. Qualitatively this is the only signal in the candidate that presents linearity between $\pm 1 \times 10^{-5}$ diopters. The slope itself around perfect mode matching is shallow. The general slope in the positive region around 1×10^{-5} diopters to 5×10^{-5} diopters is $33.84\ \mathrm{W/diopter}$.

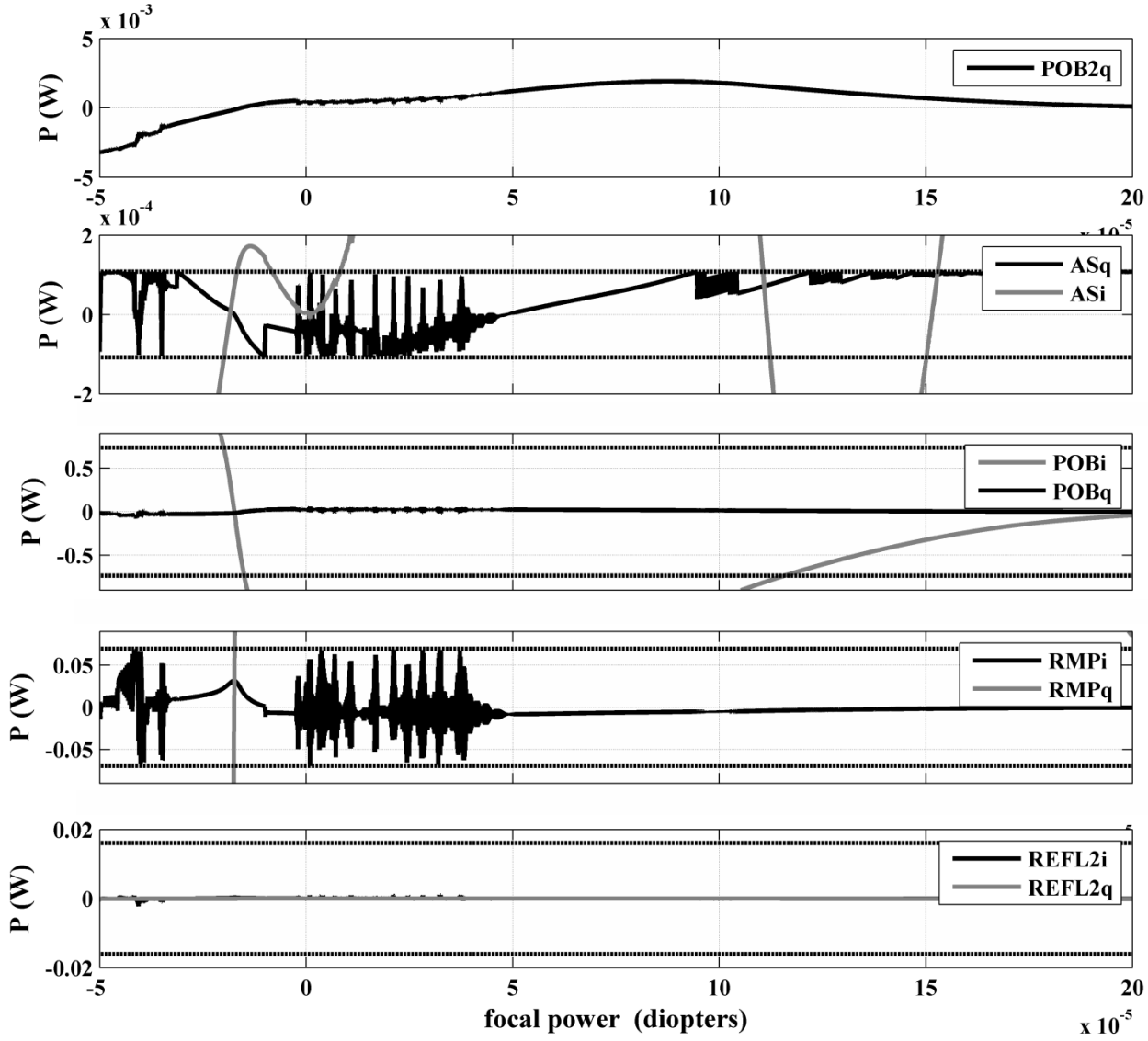

Figure 5: Differential lensing and control signals: Trace 1 shows the behaviour of the beamsplitter pickoff light demodulated in the quadrature phase at the secondary sideband modulation frequency. The signal reaches a slope of 33.84 W/diopter near $5*10^{-5}$ diopters. Somewhat flat behaviour around perfect mode matching suggests that a servo may wander out to +/- $2*10^{-5}$ diopters. This wander is negligible since this is within the plateau of maximum arm power. In the following traces, the letters "i" and "q" refer to in-phase demodulation and quadrature phase demodulation, respectively. The following traces, in order, correspond to the various degree of freedom error signals: ASq = differential arm control; POBq = the Michelson; RMPi = the common motion of the power recycling cavity; and REFL2i = the common motion of the arm cavities. The dotted lines correspond to the locking accuracy threshold or RMS motion of a specific length degree of freedom. The servos remain stable throughout the operating region from $-5*10^{-5}$ diopters to $5*10^{-5}$ diopters.

8. Necessity of a Servo

Disturbances to the LIGO interferometer's operating state, such as ground vibration and thermal drift, are reduced by use of servo controls. Such a linear servo is probably not needed here due to the lack of optically induced thermal transients during scientific operation. Nonetheless, the signal candidates provide landmarks distinctive enough for either manual or computer controlled setting of the TCS to optimize detector sensitivity. A five-hour measurement in Livingston of ITM temperature (via a substrate mechanical mode frequency) without TCS active indicates that the main disturbance that a servo would need to track is the intensity variations in the main laser beam in the recycling cavity. We estimate that only several mHz of servo bandwidth would be needed to track this, and that only 1×10^{-8} diopters (RMS) was present. The long time periods and focal power excursions are therefore so small as to not require any monitoring let alone servo control.

The process of taking a LIGO detector from its cold state to full power operation is quite complex. The stage between detector resonance acquisition and full operating power increased power by nearly eight times. This transient resulted in an ITM focal power change similar to that noted in section 6. Such a large change in focal power would advocate either a control loop or a lookup table of TCS power settings with respect to injected main laser power [4].

9. Conclusions

The ITMs serve a critical role in LIGO. When thermally loaded, they improve mode matching of the primary RF sideband within the PRC. This was of paramount importance to the S5 differential displacement detection scheme. Nonuniform heating of the ITMs generated thermal lensing. When the ITMs were suboptimally lensed LIGO's sensitivity was compromised. During S5, a means of monitoring optimal mode matching was empirically determined. However, these signals were not always reliable especially at circulating power levels beyond those used in S5. A model of the detector was composed to search for better thermal lens monitoring signals. Following a set of stipulations, a set of candidate signals were found. We also determined that there was no need for a TCS control system to optimize LIGO sensitivity during quiescent operation. Any suggested modifications to the TCS itself would be toward improving delivered intensity stability.

10. Acknowledgements

We would like to acknowledge the National Science Foundation for their support of both this research grant number PHY-0905184 and their commitment to Louisiana State University and the LIGO Lab. We would also like to acknowledge the continuing cooperation between the LIGO Lab and LSU which permits students to be actively involved with ongoing research at the observatories. LIGO was constructed by the California Institute of Technology and Massachusetts Institute of Technology with funding from the National Science Foundation and operates under cooperative agreement PHY-0757058.

References:

1. **Abramovici, A., W.E. Althouse, R.W. Drever, Y. Gursel, S. Kawamura, F.J. Raab, D. Shoemaker, L. Sievers, R.E. Spero, K.S. Thorne, et al., *LIGO: The Laser Interferometer Gravitational-Wave Observatory.* Science, 1992: p. 256.**
2. **Abbott, B., et al., *Detector Description and Performance for the First Coincidence Observations between LIGO and GEO.* Nuclear Instruments and Methods in Physics Research A, 2003. 517(1-3): p. 154-179.**
3. **Abbott, B., et al., *LIGO: The Laser Interferometer Gravitational-Wave Observatory.* Reports on Progress in Physics, July 2009. 72(7).**
4. **Ballmer, S.W., *LIGO interferometer operating at design sensitivity with application to gravitational radiometry*. 2006, Massachusetts Inst. of Technology (Dissertation).**
5. **Smith, M., D. Ottaway, P. Willems, C. Vorvick, and G. Moreno, *Heating Beam Pattern Optical Design CO2 Laser Thermal Compensation Bench (LIGO DCC T040057-01-D)*. 2004.**
6. **Betzwieser, J., *Analysis of spatial mode sensitivity of a gravitational wave interferometer and a targeted search for gravitational radiation from the Crab pulsar*. 2007, Massachusetts Institute of Technology (Dissertation).**
7. **Gretarsson, A.M., E. D'Ambrosio, V. Frolov, B. O'Reilly, and P.K. Fritsche, *Effects of mode degeneracy in the LIGO Livingston Observatory recycling cavity.* J. Opt. Soc. Am. B, 2007. 24(11): p. 2821-2828.**
8. **Lawrence, R., M. Zucker, and P. Fritschel, *Active correction of thermal lensing through external radiative thermal actuation.* Optics Letters, 2004. 29(22): p. 2635--2637.**
9. **Lawrence, R., M. Zucker, P. Fritschel, P. Marfuta, and D. Shoemaker, *Adaptive thermal compensation of test masses in advanced LIGO* Classical and Quantum Gravity, 2002. 19(7): p. 1803.**
10. **Strain, K.A., K. Danzmann, J. Mizuno, P.G. Nelson, A. Rudiger, R. Schilling, and W. Winkler, *Thermal lensing in recycling interferometric gravitational wave detectors.* Physics Letters A, 1994. 194(1-2): p. 124-132.**
11. **R. W. P. Drever, J.L. Hall, F.V. Kowalski, J. Hough, G.M. Ford, A.J. Munley, and H. Ward, *Laser Phase and Frequency Stabilization Using an Optical Resonator.* Applied Physics B, 1983. 31: p. 97-105.**
12. **Fritschel, P.K., G. Gonzalez, N. Mavalvala, D. Shoemaker, D. Sigg, and M.E. Zucker, *Alignment of an interferometric gravitational wave detector.* Applied Optics, 1998. 37(28): p. 6734-6747.**
13. **Ottaway, D., S. Ballmer, J. Betzweiser, K. Kawabe, B. Kells, M. Rahkmanov, R. Savage, and S. Waldman, *Optical absorption in Initial LIGO IFOs (LIGO DCC T050074-00-R)*. 2005.**
14. **Gretarsson, A.M., E. D'Ambrosio, V. Frolov, B. O'Reilly, and P.K. Fritschel, *Effects of mode degeneracy in the LIGO Livingston Observatory recycling cavity.* J. Opt. Soc. Am. B, 2007. 24(11): p. 2821-2828.**
15. **Lawrence, R., *Active Wavefront Correction in Laser Interferometric Gravitational-wave Detectors*. 2003: Massachusetts Inst. of Technology (Dissertation).**
16. **Winkler, W., K. Danzmann, A. Rudiger, and R. Schilling, *Heating by optical absorption and the performance of interferometric gravitational-wave detectors.* Physical Review A, 1991: p. 7022-7036.**
17. **Zucker, M., D. Ottaway, and K. Mason, *Thermal Compensator Retrofit for LIGO 1 (LIGO-T030062-03-D)*, in *LIGO DCC*. 2003, CIT.**
18. **Gretarsson, A.M. *Report on Power Increase Work*. 2004 [cited 2009 November]; Available from: http://ilog.ligo-**

la.caltech.edu/ilog/pub/ilog.cgi?group=detector&date_to_view=01/22/2004&anchor_to_scroll_to=2004:01:22:05:43:29-andri.

19. Ballmer, S., V. Frolov, R. Lawrence, W. Kells, G. Moreno, K. Mason, D. Ottaway, M. Smith, C. Vorvick, P. Willems, et al., *Thermal Compensation System Description (LIGO DCC T050064-00-R)*. 2005.
20. Mueller, G., Q.-z. Shu, R. Adhikari, D.B. Tanner, and D. Reitze, *Determination and optimization of mode matching into optical cavities by heterodyne detection.* Optics Letters, 2000. 25(4): p. 266--268.
21. Sigg, D., *Status of the LIGO detectors.* Classical and Quantum Gravity, 2008. 25: p. 114041.
22. Smith, J., *The path to the enhanced and advanced LIGO gravitational-wave detectors.* arXiv:0902.0381v2 [gr-qc], 2009.
23. Mueller, G., R.S. Amin, D. Guagliardo, D. McFeron, R. Lundock, D.H. Reitze, and D.B. Tanner, *Method for compensation of thermally induced modal distortions in the input optical components of gravitational wave interferometers.* J. Classical and Quantum Gravity, 2002: p. 1793-1801.
24. Mansell, J., J. Hennawi, E.K. Gustafson, M.M. Buyer, F. Buyer, R.L. Buyer, D. Clubley, S. Yoshida, and D.H. Reitze, *Evaluating the effect of transmissve optics thermal lensing on laser beam quality with a Shack-Hartmann wave-front sensor.* Applied Optics, vol. 40, 2001: p. 366-370.
25. A. Freise, G. Heinzel, H. Luck, R. Schilling, and K. Danzmann, *Frequency domain interferometer simulations with higher-order spatial modes.* Classical and Quantum Gravity, 2004. 21(5): p. S1067-S1074.
26. Freise, A., *Frequency domain INterferomEter Simulation SoftwarE v.0.99.8* <*http://www.gwoptics.org/finesse/*> 2009: Birmingham, U.K.
27. Hild, S., H. Luck, W. Winkler, K. Strain, H. Grote, J. Smith, M. Malec, M. Hewitson, B. Willke, J. Hough, et al., *Measurement of a low-absorption sample of OH-reduced fused silica.* Applied Optics, 2006. 45(28): p. 7269-7272.